Electronic Supplementary Material (ESI) for ChemComm.

Electronic Supplemental Information for

Air-fabricated $CsPbIBr_2$ perovskite film for efficient and stable solar cells by triacetyl resveratrol additive

Jiabao Li,[a,b] Ziting Qi,[a] Peizhi Yang,*[,a] Qunwei Tang*[,b] and Jialong Duan*[b,c]

[a] Key Laboratory of Advanced Technique & Preparation for Renewable Energy Materials, Ministry of Education, Yunnan Normal University, Kunming 650500, P. R. China;

[b] Institute of Carbon Neutrality, College of Chemical and Biological Engineering, Shandong University of Science and Technology, Qingdao 266590, P. R. China;

[c] Wuhan National Laboratory for Optoelectronics and School of Physics, Huazhong University of Science and Technology, Wuhan 430074, P. R. China

*E-mail address: pzhyang@hotmail.com; tangqunwei@sdust.edu.cn; duanjialong@sdust.edu.cn;

Experimental Section

Materials and Reagents: Cesium iodide (CsI, 99.99%) and Triacetyl resveratrol (TRES, ≥ 98%) were purchased from Aladdin. Lead bromide ($PbBr_2$, 99.99%), titanium (IV) isopropoxide (99.9%), diethanol amine (DEA, 99%), anhydrous dimethyl sulfoxide (DMSO, 99.7%), isopropanol (IPA, ≥ 99.5%) and ethanol (EtOH, 99.7%) were purchased from Macklin. Lead iodide (PbI_2, 99.99%) were obtained from Xi'an Polymer Light Technology Co., Ltd. Zinc powder, acetone (Ace) and hydrochloric acid (HCl) were obtained from AR Guangzhou Chemical Reagent Factory. Commercial carbon paste was obtained from Shanghai MaterWin New Materials (MTW-CE-C-003, ~10 Ω sq^{-1}). Fluorine-doped tin oxide-coated (FTO) substrates with a sheet resistance of 14 Ω sq^{-1} were purchased from Pilkington. Unless mentioned otherwise, all the materials and reagents were commercially purchased and used as received free of further purification.

Device Fabrication: Perovskite solar cells were fabricated onto a FTO glass substrate. FTO was firstly etched with desired pattern via zinc powder and hydrochloric acid and then consecutively washed with deionized water, acetone, isopropanol and ethanol in an ultrasonic bath for 30 min, respectively, and finally treated with UV–ozone for 180 s. A compact titanium dioxide layer (c-TiO_2) was prepared by spin-coating a solution (0.5 M diethanol amine and 0.5 M titanium isopropoxide ethanol solution, respectively) at 7000 rpm for 30 s, and then annealed at 500 ℃ for 2 h in air. The obtained FTO/c-TiO_2 substrates were treated with UV–ozone for another 180 s. For $CsPbIBr_2$-TRES perovskite layer, the 80 μL of 1.0 M $CsPbIBr_2$ precursor solution containing 260 mg of CsI, 367 mg of $PbBr_2$, 4.6 mg of PbI_2 and desired content (0 mol%, 0.1 mol%, 0.3 mol%, 0.5 mol%) TRES dissolved in 1 mL of DMSO was spin-coated onto FTO/c-TiO_2 substrate at 1000 rpm for 10 s and then 3000 rpm for 30 s in ambient air. The crystallization process of perovskite thin film includes a two-step thermal treatment process. In detail, At the 5nd second of the first step of spin-coating, a hot flow of 100 °C was blown on the substrate until

the color of the film turned yellow. The distance between the muzzle of hot-air gun (858D, DongGuan BuFan Electronics Co,. LTD) and the substrate was nearly 4 cm. The whole blowing process lasted about 20 s. Afterward, the substrate was placed on a hotplate at 150 °C for 1 min and then at 260 °C for 10 min and cooled down to room temperature naturally. Similarly, the $CsPbI_2Br$ perovskite layer was also deposited via a two-step thermal treatment process as previously reported.[1] Briefly, the 80 µL of 1.2 M $CsPbI_2Br$ precursor solution containing 312 mg of CsI, 220 mg of $PbBr_2$, 277 mg of PbI_2 and desired content (0 mol%, 0.3 mol%) TRES dissolved in 1 mL of DMSO was spin-coated onto FTO/c-TiO_2 substrate at 1000 rpm for 10 s and then 3000 rpm for 30 s in ambient air. At the 5nd second of the first step of spin-coating, a hot flow of 100 °C was blown on the substrate until the color of the film turned brown. The distance between the muzzle of hot-air gun (858D, DongGuan BuFan Electronics Co,. LTD) and the substrate was nearly 4 cm. The whole blowing process lasted about 20 s. Afterward, the substrate was placed on a hotplate at 160 °C for 1 min and then at 270 °C for 10 min and cooled down to room temperature naturally. Finally, the commercial carbon paste was bladed onto the as-prepared substrate with an active area of 0.09 cm^2 and then dried at 200 °C for 2 min.

Characterizations and Measurements: The morphologies characterizations of samples were conducted by scanning electron microscopy (SEM, Regulus8100, JAPAN). The X-ray photoelectron spectroscopy (XPS) spectra were measured via a RBD upgraded PHI-5000C ESCA system (Perkin Elmer) equipped with Mg *K*α as the X-ray source (*h*ν = 1253.6 eV). The crystallinity of perovskite films was determined by the X-ray diffraction (XRD, Bruker D8 ADVANCE) with Cu Kα (*λ* = 1.5406 Å) radiation at 40 kV and 40 mA. KPFM images were captured using an AFM system (Multimode 8, Bruker, German). The optical absorption spectra of perovskite films were characterized by UV-vis spectrophotometer (UV-8000A) under the wavelength range of 300 ~ 800 nm. The steady-state photoluminescence (PL) spectra and time-resolved photoluminescence (TRPL) spectra were obtained on a FluoroMax-4 spectrofluorometer

and a Horiba spectrometer under excitation wavelength of 410 nm and 470 nm, respectively. The external quantum efficiency (EQE, QE-R) spectra of devices were obtained by a IPCE kit developed by Enli Technology Co., Ltd with a standard Si crystalline solar cell as a reference. The current density-voltage (*J-V*) curves of solar cells were measured on an electrochemical workstation (CHI660E) under standard solar irradiation (Newport, Oriel Class A, 91195A, AM 1.5G ,100 mW cm^{-2}, calibrated by a standard silicon solar cell) equipped with 500 W Xenon lamp. The steady-state output of photocurrent and PCE were measured via a Keithley 2420 digital source meter under a certain bias. The Urbach energy (E_U) of film was calculated by probing the direct absorption band edge. According to the equation: $\alpha = \alpha_0 \exp(h\nu/E_U)$, in which α is the absorption coefficient, α_0 is a constant and E_U represents the photon energy. The trap state density (N_t) was calculated according to the space-charge-limited current (SCLC) method equation: $N_t = 2\varepsilon_0\varepsilon_r V_{TFL}/eL^2$, where V_{TFL} is the onset voltage of the trap-filled limit, e is the elementary charge of an electron, L is the thickness of the perovskite film, and ε_0 is the vacuum permittivity and ε_r the relative dielectric constant. The electrochemical impedance spectroscopy (EIS) measurements, the open-circuit voltage (V_{OC}) decay curves, and the Mott–Schottky plots, tafel curves were conducted on the CHI660E electrochemical workstation. All the moisture and thermal durability under working conditions as well as the long-term stability were measured on the devices without encapsulation.

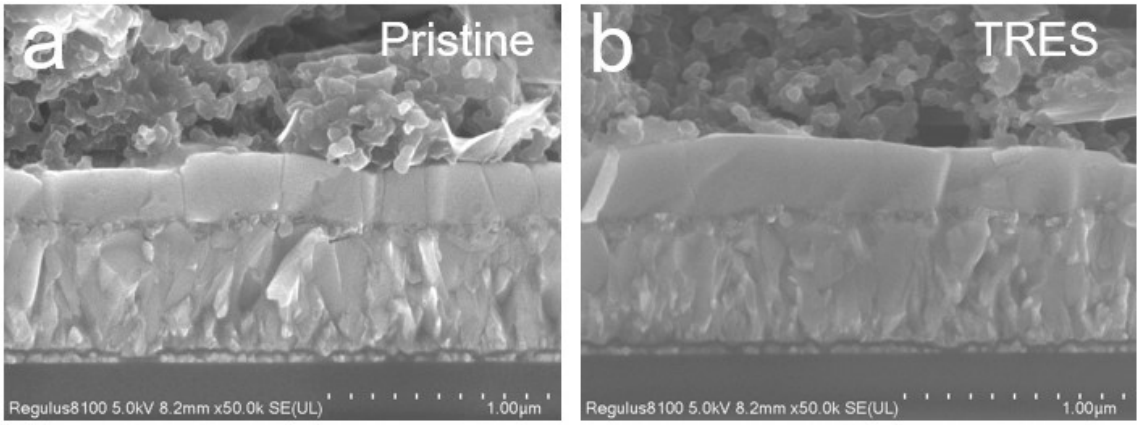

Figure S1. The cross-sectional SEM images of (a) pristine and (b) TRES-treated inorganic $CsPbIBr_2$ PSCs.

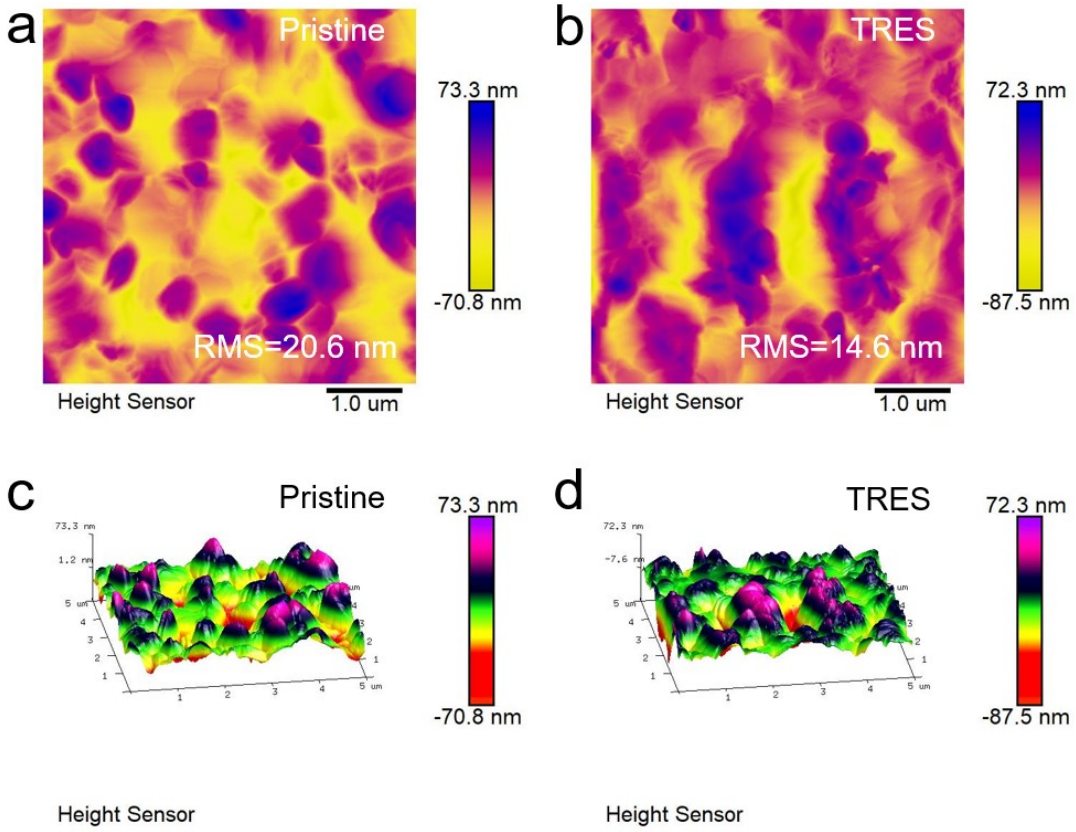

Figure S2. AFM height images of films (a) pristine and (b) 0.3 mol% TRES-doped. Three-dimensional AFM height images of perovskite films (c) pristine and (d) 0.3 mol% TRES-doped.

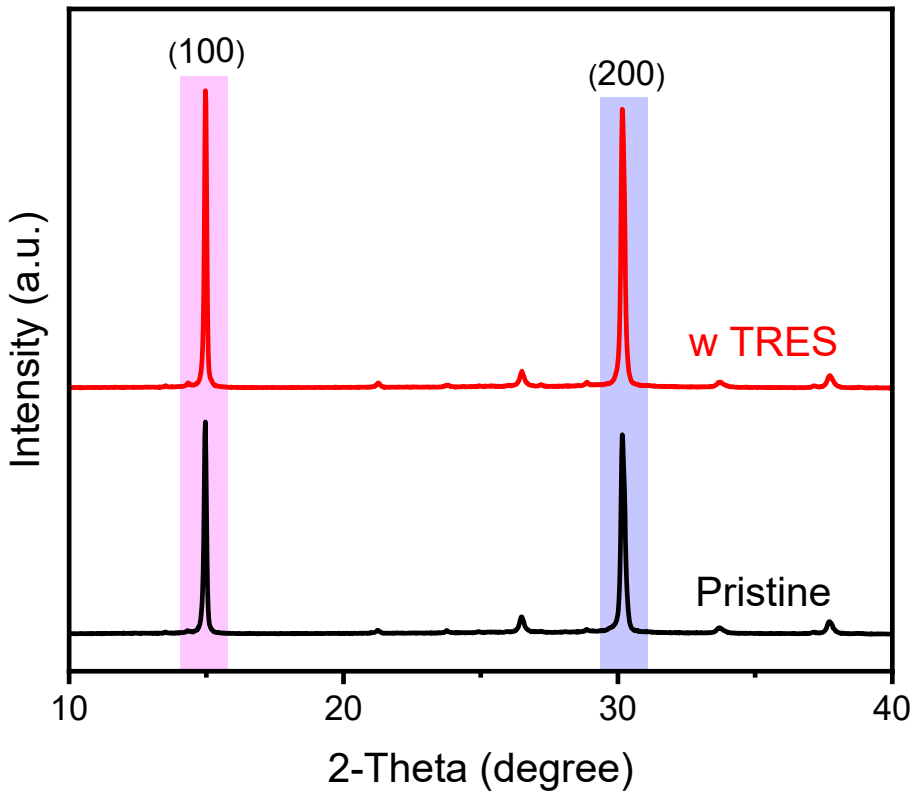

Figure S3. XRD patterns of $CsPbIBr_2$ perovskite films with and without TRES modification.

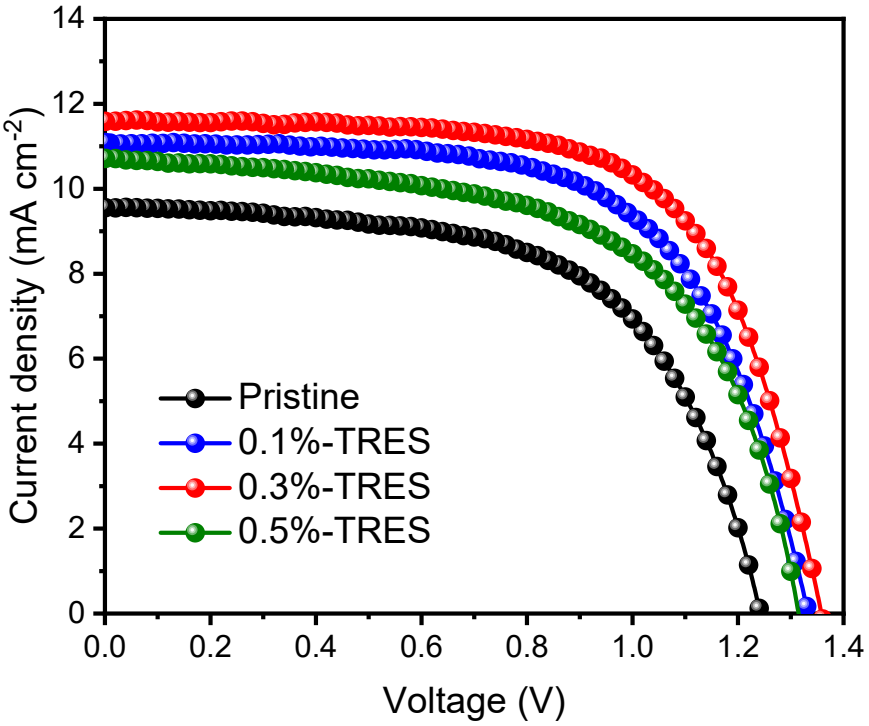

Figure S4. Best-performing *J-V* curves under reverse scanning direction of $CsPbIBr_2$ constructed PSCs tailored with different TRES concentrations.

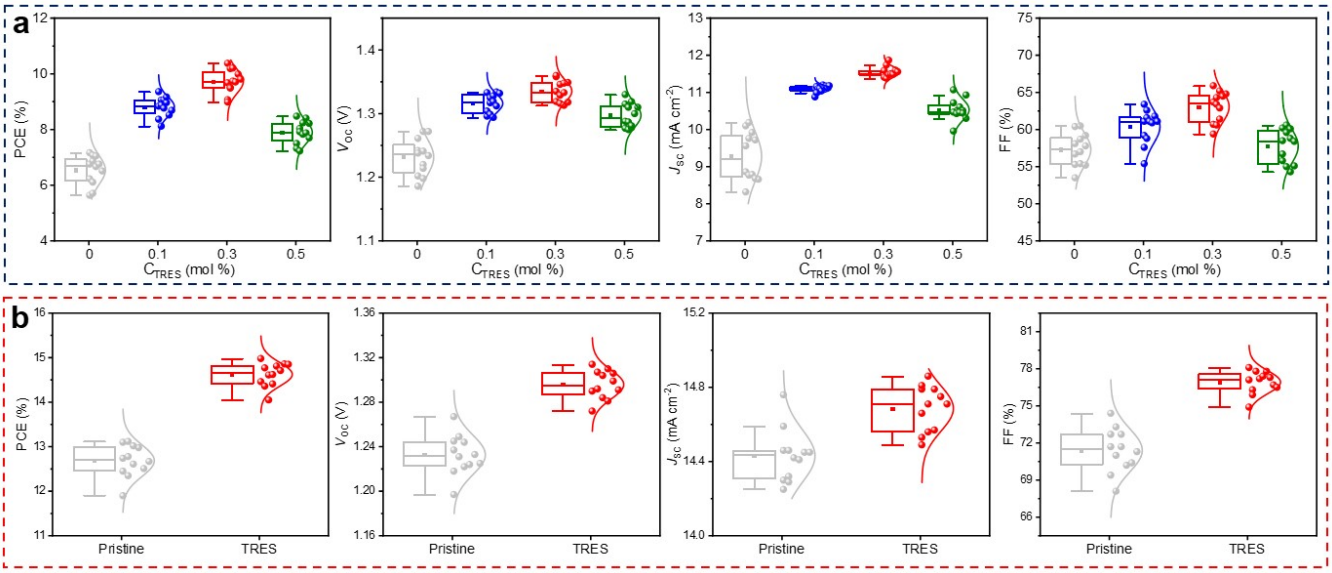

Figure S5. Statistical PCE, V_{OC}, J_{SC}, and FF values of (a) $CsPbIBr_2$ constructed PSCs tailored with different TRES concentrations. Statistical PCE, V_{OC}, J_{SC}, and FF values of (b) pristine and TRES treated $CsPbI_2Br$ PSC. Each average photovoltaic parameter was obtained from 12 devices to check the reproducibility.

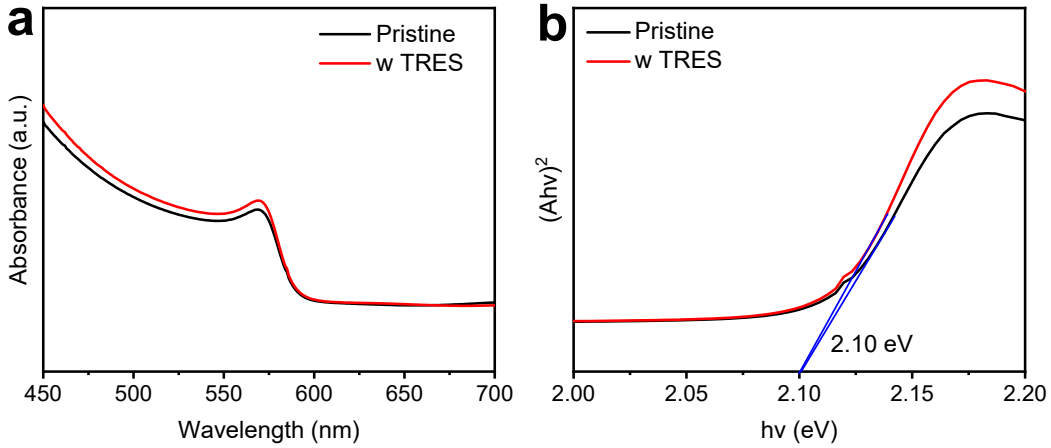

Figure S6. (a) UV-vis absorption spectra of pristine and TRES-treated films. (b) Tauc-plot curves of perovskite films with and without TRES treatment.

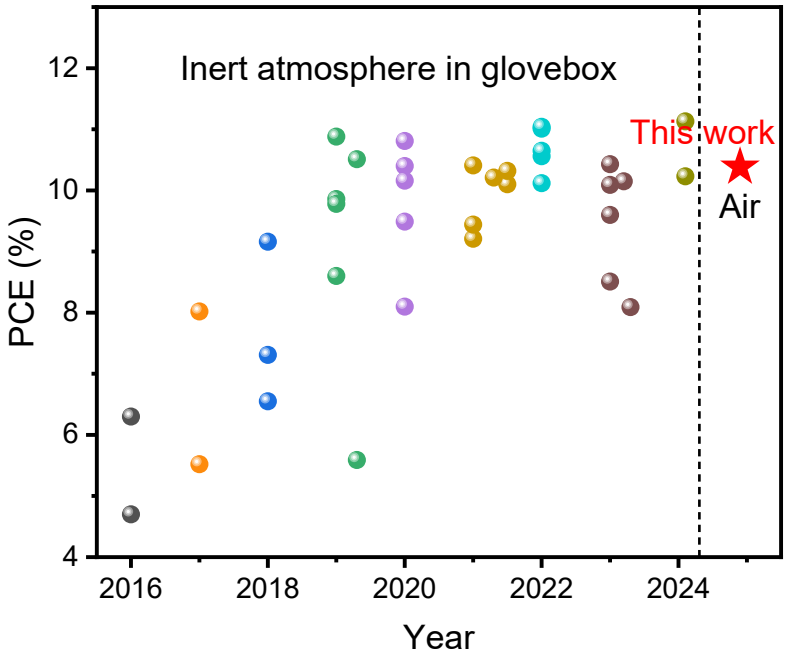

Figure S7. Summary of photovoltaic performances for $CsPbIBr_2$ structured PSCs.

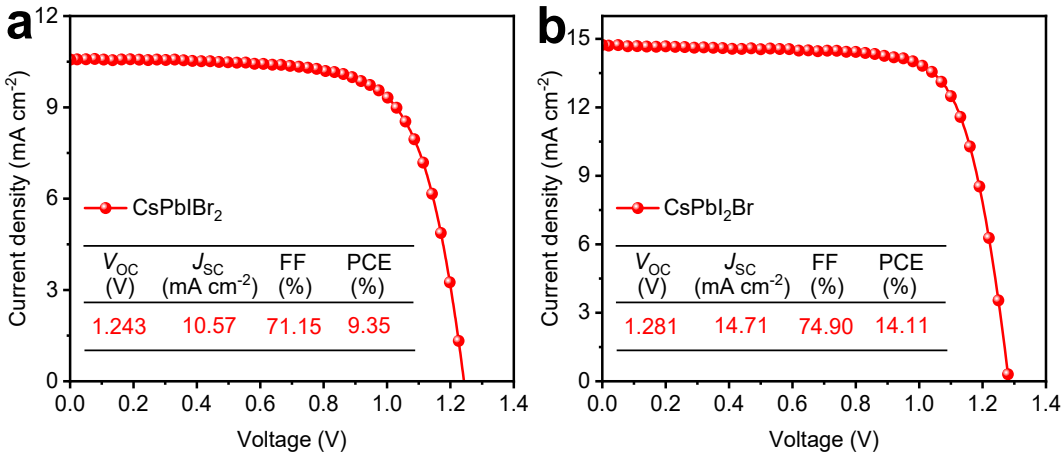

Figure S8. *J-V* curves of (a) $CsPbIBr_2$ and (b) $CsPbI_2Br$ PSCs fabricated in inert environment.

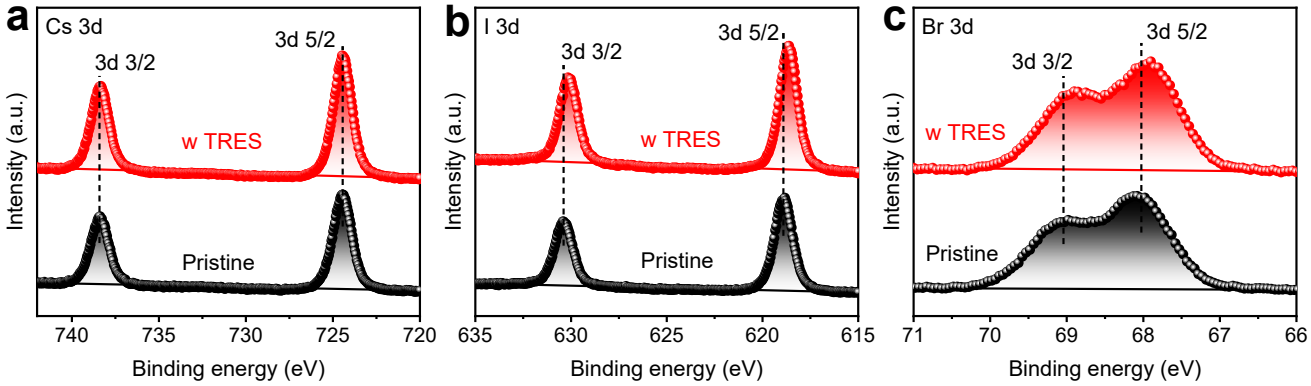

Figure S9. XPS spectra of (a) Cs 3d, (b) I 3d and (c) Br 3d for perovskite films without and with TRES doped.

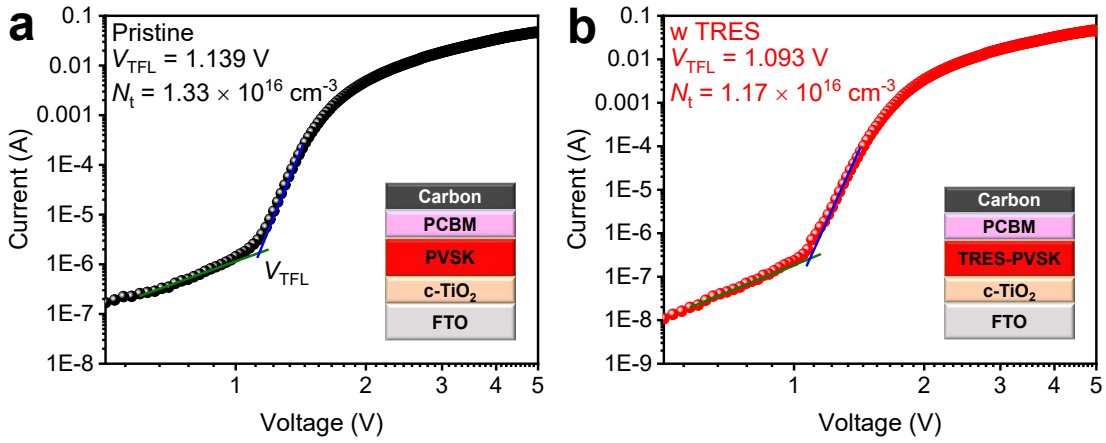

Figure S10. Dark *J-V* curves of the electron-only devices (FTO/c-TiO_2/perovskite/PCBM/carbon) based on pristine and TRES-treated perovskites.

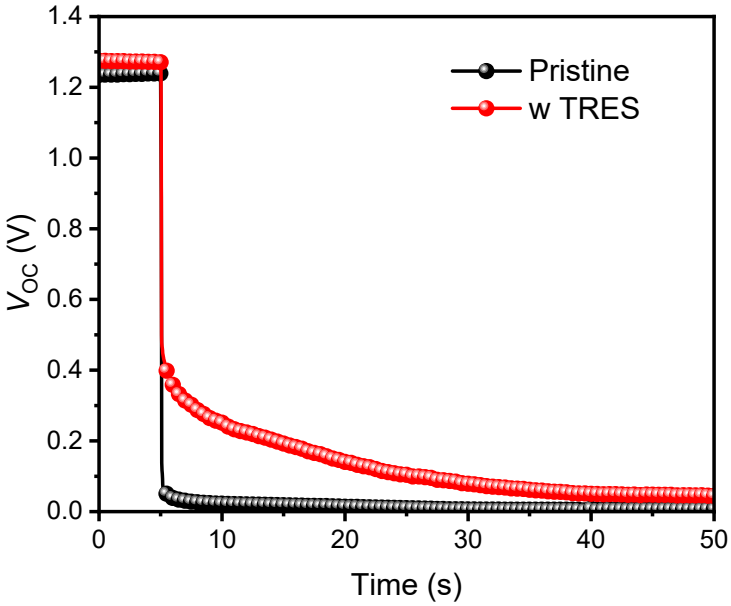

Figure S11. Open-circuit voltage decay curves of pristine and TRES-doped PSCs.

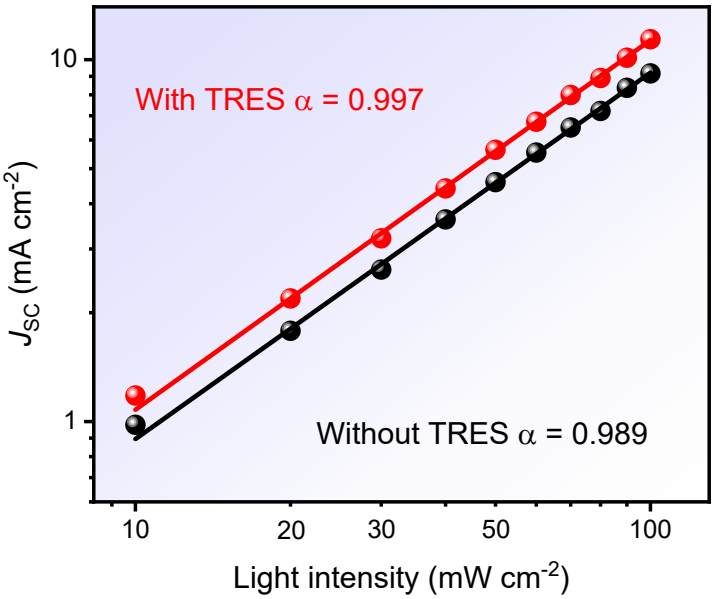

Figure S12. The dependence of J_{SC} on light intensity for device with and without TRES treated.

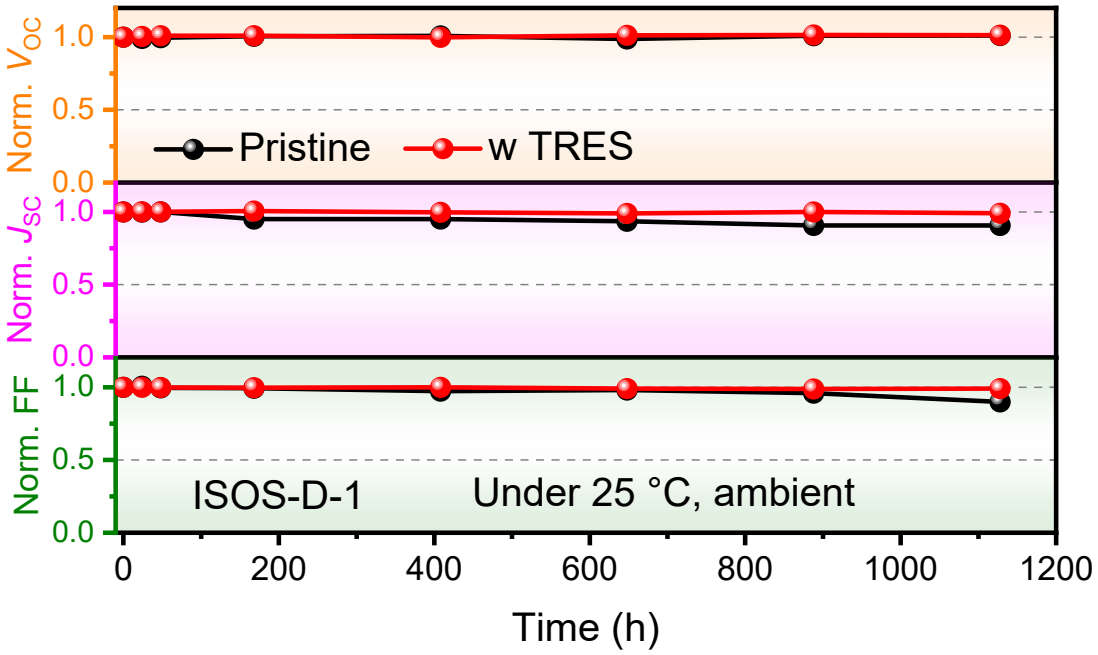

Figure S13. Long-term stability of pristine and TRES-tailored devices stored under ambient condition with 30% RH without encapsulation (ISOS-D-1).

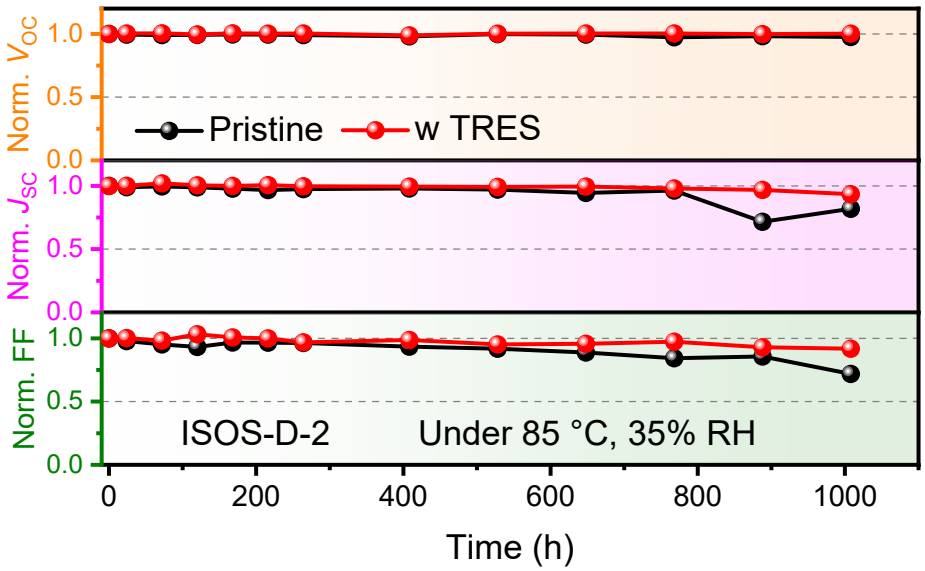

Figure S14. Thermal stability of unencapsulated PSCs stored at 85 °C and 35% RH (ISOS-D-2).

Table S1. The photovoltaic parameters of $CsPbIBr_2$ PSCs with different concentrations of MWCNT-doped under standard illumination.

C_{TRES}	J_{sc} (mA cm^{-2})	V_{oc} (V)	FF (%)	PCE (%)
Pristine	9.56	1.242	60.4	7.17
0.1 mol%	11.09	1.333	63.4	9.36
0.3 mol%	11.59	1.358	65.9	10.38
0.5 mol%	10.72	1.315	60.2	8.48

Table S2. Photovoltaic data of the without and with TRES-doped PSCs.

Perovskites	Doped	J_{SC} (mA cm^{-2})	V_{OC} (V)	FF (%)	PCE (%)	HI[a] (%)
$CsPbIBr_2$	Pristine	9.56/9.35	1.242/1.176	60.4/47.9	7.17/5.27	26.50
	w TRES	11.59/11.52	1.358/1.335	65.9/58.5	10.38/8.99	13.39
$CsPbI_2Br$	Pristine	14.46/14.34	1.245/1.183	72.7/64.3	13.10/10.91	16.72
	w TRES	14.79/14.68	1.314/1.268	77.1/73.2	14.98/13.63	9.01

[a])Hysteresis index (HI) obtained from the following equation: HI = (PCER-PCEF)/PCER.

Table S3. Summary of the photovoltaic data and V_{loss} for previously reported $CsPbIBr_2$.

Device architecture	*Eg* (eV)	V_{loss} (V)	J_{SC} (mA cm^{-2})	V_{OC} (V)	FF (%)	PCE (%)	Ref.
Based on $CsPbIBr_2$							
FTO/c-TiO_2/$CsPbIBr_2$-TRES/Carbon	**2.10**	**0.742**	**11.59**	**1.358**	**65.90**	**10.38**	**This work**
FTO/c-TiO_2/PMMA-$CsPbIBr_2$/Carbon	2.10	0.793	11.36	1.307	62.00	9.21	2
FTO/c-TiO_2/$CsPbIBr_2$-FAAc/Spiro-OMeTAD/Au	2.05	0.93	11.65	1.12	72.39	9.44	3
ITO/c-TiO_2/$CsPbIBr_2$/quinoline sulfate/Carbon	2.08	0.782	11.53	1.298	69.59	10.41	4
FTO/c-TiO_2/$CsPbIBr_2$-NH_4PF_6/Spiro-OMeTAD/Au	2.10	0.97	12.11	1.13	74.00	10.10	5
FTO/c-TiO_2/$CsPbIBr_2$/Carbon	2.10	0.773	11.43	1.327	69.70	10.56	6
FTO/TiO_2/$CsPbIBr_2$/Carbon	2.10	0.83	10.99	1.27	58.00	8.10	7
FTO/c-TiO_2/$CsPbIBr_2$-Cu/Spiro-OMeTAD/Ag	2.05	0.84	12.80	1.21	67.10	10.40	8
ITO/SnO_2/$CsPbIBr_2$/Spiro-OMeTAD/Ag	2.10	0.83	11.91	1.27	71.72	10.81	9
ITO/ZnO/$CsPbIBr_2$/Spiro-OMeTAD/Au	2.05	0.761	11.34	1.289	75.31	11.01	10
FTO/$CsNiO_x$/N749/$CsPbIBr_2$/ PCBM/BCP/Ag	2.05	0.86	11.49	1.19	69.00	9.49	11
FTO/c-TiO_2/$CsPbIBr_2$/Carbon	2.05	0.77	11.17	1.28	60.00	8.60	12
FTO/TiO_2/$SmBr_3$/Sm-$CsPbIBr_2$/Spiro-OMeTAD/Au	2.06	0.89	12.75	1.17	73.00	10.88	13
FTO/c-TiO_2/$CsPbIBr_2$/Carbon	2.05	0.81	10.66	1.24	69.00	9.16	14
FTO/c-TiO_2/$CsPbIBr_2$-PEG/Spiro-OMeTAD/Au	2.07	0.79	8.80	1.28	64.90	7.31	15
FTO/c-TiO_2/$CsPbIBr_2$/Carbon	2.05	0.91	9.11	1.14	63.00	6.55	16
FTO/c-TiO_2/$CsPbIBr_2$/Spiro-OMeTAD/Au	2.10	0.87	9.69	1.23	67.40	8.02	17
FTO/c-TiO_2/mp-TiO_2/$CsPbIBr_2$/Spiro-OMeTAD/Au	2.05	0.92	7.80	1.13	72.00	6.30	18
FTO/NiO_x/$CsPbIBr_2$/MoO_x/Au	2.05	1.20	10.56	0.85	62.00	5.52	19
FTO/c-TiO_2/$CsPbIBr_2$/Carbon	2.05	1.09	8.70	0.96	56.00	4.70	20
FTO/c-TiO_2/$Cs_xK_{1-x}PbIBr_2$/Spiro-OMeTAD/Au	2.10	0.84	9.36	1.26	73.00	8.51	21
ITO/TiO_2/ODTC-$CsPbIBr_2$/Carbon	2.05	0.75	11.48	1.30	68.00	10.15	22
ITO/TiO_2/$CsPbIBr_2$/$Ti_3C_2Cl_x$/Carbon	2.11	0.82	11.56	1.29	69.93	10.43	23
FTO/SnO_2/$CsPbIBr_2$/Spiro-OMeTAD/Au	2.09	0.85	10.79	1.24	71.68	9.60	24
ITO/SnO_2/$CsPbIBr_2$/Spiro-OMeTAD/Ag	2.07	0.803	10.69	1.267	71.00	9.86	25
ITO/SnO_2/CsXth-$CsPbIBr_2$/P3HT/Au	2.05	0.75	10.19	1.30	73.81	9.78	26
FTO/In_2S_3/$CsPbIBr_2$/Spiro-OMeTAD/Ag	2.08	0.99	7.76	1.09	65.94	5.59	27
FTO/TiO_2/CsPb(Ba)IBr_2/Spiro-OMeTAD/Au	2.11	0.92	11.91	1.19	74.00	10.51	28
ITO/ZnO-NH_4Cl/$CsPbIBr_2$/Spiro-OMeTAD/Ag	2.07	0.80	11.52	1.27	69.17	10.16	29

FTO/c-TiO_2/m-TiO_2/PTU-$CsPbIBr_2$/Carbon	2.10	0.84	11.28	1.26	71.00	10.09	30
FTO/Li: TiO_2/$CsPbIBr_2$/Carbon	2.05	0.79	10.01	1.26	64.00	8.09	31
FTO/TiO_2/$CsPbIBr_2$/$Zn(DDTC)_2$/Carbon	2.11	0.792	11.60	1.318	66.75	10.21	32
FTO/c-TiO_2/$CsPbIBr_2$/$CsPbI_3$ QDs/Spiro-OMeTAD/Au	2.10	0.90	11.09	1.20	77.70	10.32	33
ITO/TiO_2/$CsPbIBr_2$ ($Zn(Ac)_2$)/Carbon	2.10	0.81	11.79	1.29	69.93	10.65	34
FTO/c-TiO_2/$CsPbIBr_2$/ZrO_2/Carbon	2.10	0.79	11.027	1.310	70.08	10.12	35
FTO/c-TiO_2/$CsPbIBr_2$/Bpy/Carbon	2.10	0.799	11.77	1.301	72.00	11.04	36
ITO/TiO_2/$CsPbIBr_2$/2-IDA/Carbon	2.10	0.79	11.64	1.31	67.11	10.23	37
FTO/c-TiO_2/ET/$CsPbIBr_2$/Carbon	2.10	0.775	11.63	1.325	72.23	11.13	38

Table S4. Fitted data from the TRPL spectra.

TRES-treated	τ_1 (ns)	a_1 (%)	τ_2 (ns)	a_2 (%)	τ_{ave} (ns)
Pristine	0.748	37.29	9.116	62.71	1.763
w TRES	0.832	29.73	13.714	70.27	2.447

References

1 G. Zhang, J. Zhang, Z. Yang, Z. Pan, H. Rao and X. Zhong, *Adv. Mater.*, 2022, **34**, 2206222.

2 W. Chai, J. Ma, W. Zhu, D. Chen, H. Xi, J. Zhang, C. Zhang and Y. Hao, *ACS Appl. Mater. Inter.*, 2021, **13**, 2868–2878.

3 Z. Chen, Q. Wang, Y. Xu, R. Zhou, L. Zhang, Y. Huang, L. Hu, M. Lyu and J. Zhu, *ACS Appl. Mater. Inter.*, 2021, **13**, 24654–24661.

4 D. Wang, W. Li, X. Liu, G. Li, L. Zhang, R. Li, W. Sun, J. Wu and Z. Lan, *ACS Appl. Energy Mater.*, 2021, **4**, 5747–5755.

5 J. Pan, X. Zhang, Y. Zheng and W. Xiang, *Sol. Energ. Mat. Sol. C.*, 2021, **221**, 110878.

6 F. Yan, P. Yang, J. Li, Q. Guo, Q. Zhang, J. Zhang, Y. Duan, J. Duan and Q. Tang, *Chem. Eng. J.*, 2022, **430**, 132781.

7 G. Wang, J. Liu, M. Lei, W. Zhang and G. Zhu, *Electrochim. Acta*, 2020, **349**, 136354.

8 P. Liu, X. Yang, Y. Chen, H. Xiang, W. Wang, R. Ran, W. Zhou and Z. Shao, *ACS Appl. Mater. Inter.*, 2020, **12**, 23984–23994.

9 S. Cao, H. Wang, H. Li, J. Chen and Z. Zang, *Chem. Eng. J.*, 2020, **394**, 124903.

10 J. Huang, S. He, W. Zhang, A. Saparbaev, Y. Wang, Y. Gao, L. Shang, G. Dong, L. Nurumbetova and G. Yue, *Sol. RRL*, 2022, **6**, 2100839.

11 S. Yang, L. Wang, L. Gao, J. Cao, Q. Han, F. Yu, Y. Kamata, C. Zhang, M. Fan, G. Wei and T. Ma, *ACS Appl. Mater. Inter.*, 2020, **12**, 13931–13940.

12 Q. Zhang, W. Zhu, D. Chen, Z. Zhang, Z. Lin, J. Chang, J. Zhang, C. Zhang and Y. Hao, *ACS Appl. Mater. Inter.*, 2019, **11**, 2997–3005.

13 W. S. Subhani, K. Wang, M. Du, X. Wang and S. Liu, *Adv. Energy Mater.*, 2019, **9**, 1803785.

14 W. Zhu, Q. Zhang, D. Chen, Z. Zhang, Z. Lin, J. Chang, J. Zhang, C. Zhang and Y. Hao, *Adv. Energy Mater.*, 2018, **8**, 1802080.

15 J. Lu, S.-C. Chen and Q. Zheng, *ACS Appl. Energy Mater.*, 2018, **1**, 5872–5878.

16 W. Zhu, Q. Zhang, C. Zhang, Z. Zhang, D. Chen, Z. Lin, J. Chang, J. Zhang and Y. Hao, *ACS Appl. Energy Mater.*, 2018, **1**, 4991–4997.

17 W. Li, M. U. Rothmann, A. Liu, Z. Wang, Y. Zhang, A. R. Pascoe, J. Lu, L. Jiang, Y. Chen, F. Huang, Y. Peng, Q. Bao, J. Etheridge, U. Bach and Y.-B. Cheng, *Adv. Energy Mater.*, 2017, **7**, 1700946.

18 Q. Ma, S. Huang, X. Wen, M. A. Green and A. W. Y. Ho-Baillie, *Adv. Energy Mater.*, 2016, **6**, 1502202.

19 C. Liu, W. Li, J. Chen, J. Fan, Y. Mai and R. E. I. Schropp, *Nano Energy*, 2017, **41**, 75–83.

20 C. F. J. Lau, X. Deng, Q. Ma, J. Zheng, J. S. Yun, M. A. Green, S. Huang and A. W. Y. Ho-Baillie, *ACS Energy Lett.*, 2016, **1**, 573–577.

21 Q. Guo, T. Zhang, W. Li, W. Li, W. Tan, D. McMeekin, Z. Xu, X.-Y. Fang, C. R. McNeill, J. Etheridge and U. Bach, *ACS Energy Lett.*, 2023, **8**, 699−706.

22 X. Liu, Y. Jing, C. Wang, X. Wang, R. Li, Y. Xu, Z. Yan, H. Zhang, J. Wu and Z. Lan, *Adv. Mater. Interfaces*,2023, **10**, 2202159.

23 Y. Xu, H. Zhang, Y. Jing, X. Wang, J. Gan, Z. Yan, X. Liu, J. Wu and Z. Lan, *Appl. Surf. Sci.*, 2023, **619**, 156674.

24 G. Sheng, Y. Zhao, J. Zheng, L. Chen, B. Qiu, L. Zhong, Y. Zhu, G. Xu and X. Xiao, *Energy Technol.*, 2023, **11**, 2200544.

25 Y. Guo, X. Yin, J. Liu and W. Que, *J. Mater. Chem. A*, 2019, **7**, 19008–19016.

26 Z.Wang, A. K. Baranwal, M. A. kamarudin, c. h. Ng, M. Pandey, T. Ma and S. Hayase, *Nano Energy*, 2019, **59**, 258–267.

27 B. Yang, M. Wang, X. Hu, T. Zhou and Z. Zang, *Nano Energy*, 2019, **57**, 718–727.

28 W. S. Subhani, K. Wang, M. Du and S. Frank Liu, *Nano Energy*, 2019, **61**, 165–172.

29 H. Wang, S. Cao, B. Yang, H. Li, M. Wang, X. Hu, K. Sun and Z. Zang, *Sol. RRL*, 2020, **4**, 1900363.

30 J. Bi, J. Chang, M. Lei, F. Meng and G. Wang, *Energy Technol.*, 2023, 2201459.

31 F. Zhao, Y. Guo, P. Yang, J. Tao, J. Jiang and J. Chu, *J. Alloy. Compd.*, 2023, **930**, 167377.

32 X. Liu , Y. Jing , R. Li , D. Wang , C. Wang , Z. Yan , W. Sun , J. Wu and Z. Lan, *J. Power Sources*, 2021, **516**, 230675.

33 Y. Xu, Q. Wang, L. Zhang, M. Lyu, H. Lu, T. Bai, F. Liu, M. Wang and J. Zhu, *Sol. RRL*, 2021, **5**, 2100669.

34 D. Wang, W. Li, T. Zhang, X. Liu, X. Jin, B. Xu, D. Li, Z. Huang, Q. Li, Z. Lan and J. Wu, *ACS Appl. Energy Mater.*, 2022, **5**, 2720−2726.

35 J. Zhang, Q. Guo, Y. Zhao, J. Duan and Q. Tang, *Chem. Commun.*, 2022, **58**, 13891–13894.

36 J. Zhang, J. Duan, Q. Zhang, Q. Guo, F. Yan, X. Yang, Y. Duan and Q. Tang, *Chem. Eng. J.*, 2022, **431**, 134230.

37 Y. Xu, H. Zhang, F. Liu, R. Li, Y. Jing, X. Wang, J. Wu, J. Zhang and Z. Lan, Appl. Surf. Sci., 2024, **658**, 159831.

38 Z. Qi, J. Li, X. Zhang, J. Dou, Q. Guo, Y. Zhao, P. Yang, Q. Tang and J. Duan, ACS Appl. Mater. Interfaces, 2024, **16**, 14974–14983.